

## Supplementary Information

# Engineering nitrogen-doped porous carbon positive electrode for high-performance sodium-ion capacitors: the critical role of porosity, structure and surface functionalities

Ademola Adeniji<sup>a,b,c</sup>, Adrian Beda<sup>a,b,c</sup>, Philippe Fioux<sup>a,b</sup>, and Camelia Matei Ghimbeu<sup>a,b,c,\*</sup>

<sup>a</sup>Université de Haute-Alsace, Institut de Science des Matériaux de Mulhouse (IS2M), CNRS  
UMR 7361, F-68100 Mulhouse, France.

<sup>b</sup>Université de Strasbourg, F-67081 Strasbourg, France.

<sup>c</sup>Réseau sur le Stockage Electrochimique de l’Energie, CNRS FR3459, 80039 Amiens,  
France.

Corresponding author: \*E-mail: [camelia.ghimbeu@uha.fr](mailto:camelia.ghimbeu@uha.fr)

## 1 Experimental method

### 1.1 Physicochemical characterization

#### 1.1.1 N<sub>2</sub> Adsorption

The specific surface area (SSA) was calculated by the Brunauer-Emmett-Teller (BET) model from the linear dependence at relative pressures ranging from 0.01 to 0.05. The micropore volume ( $V_{\text{micro}}$ ) was determined using Dubinin-Radushkevich model. The mesopore volume ( $V_{\text{meso}}$ ) was determined by subtracting the “ $V_{\text{micro}}$ ” from the total pore volume of N<sub>2</sub> adsorbed at a relative pressure (P/P<sub>0</sub>) of 0.99. The pore size distribution (PSD) was determined from the adsorption axis of the N<sub>2</sub> isotherm. The two-dimensional non-local density functional theory (2D-NLDFT) heterogeneous surface model for carbon materials @ 77 K was used on SAIEUS (Micromeritics).<sup>1</sup> The average micropore ( $L_{0\text{-}\text{micro}}$ ) and mesopore diameter ( $L_{0\text{-}\text{meso}}$ ) were determined as reported elsewhere.<sup>2</sup>

#### 1.1.2 TPD-MS

The measurements of functional groups determined by TPD-MS were performed using a procedure described elsewhere.<sup>3</sup> Briefly, the NDPC were thermally treated under a secondary vacuum (10<sup>-7</sup> Torr) up to 950 °C at a heating rate of 5 °C min<sup>-1</sup>, while the released gases due to the decomposition of functional groups were continually followed by a mass spectrometer. The total amount of each released gas was evaluated by time integration of the TPD curves. For the CO and CO<sub>2</sub> gas profile deconvolution, the full width at half maximum (FWHM), position, and area of the anhydride peaks in the CO and CO<sub>2</sub> profiles were preserved. A Gaussian model was used for peak fitting across all NDPC materials.<sup>4,5</sup> The CO<sub>2</sub> groups were deconvoluted into three main peaks (Figure S4b): two peaks corresponding to strong and weak carboxylic acids (100 – 500 °C) and a third peak corresponding to anhydrides (400 – 650 °C). The CO groups were deconvoluted (Figure S4c) mainly into anhydrides, phenol/ethers (550 – 850 °C), and

carbonyl/quinones (750 – 950 °C). Furthermore, TPD-MS facilitated the quantification of active sites by assessing the active surface area (ASA). The ASA was determined after O<sub>2</sub> chemisorption at 150 °C for 10 h,<sup>5</sup> considering the amount of CO and CO<sub>2</sub> released and the area of the carbon edge site.<sup>3</sup>

## 1.2 Electrochemical calculations

The Dunn method<sup>6</sup> is evaluated using the power law equation given by:

$$I(v) = k_1v + k_2v^{1/2} \quad (1)$$

Where "v" is the scan rate, and  $k_1v$  and  $k_2v^{1/2}$  are the capacitive effect (or pseudocapacitive) and diffusion-controlled behavior, respectively. The value of  $k_1$  and  $k_2$  are obtained by plotting  $I/v^{1/2}$  versus  $v^{1/2}$ .

The formula below were used for the evaluation of the energy and power density:<sup>7-9</sup>

$$E = \frac{1}{2} \times C \times (V_2^2 - V_1^2) \quad (2)$$

$$C = \frac{I}{\frac{dV}{dt} \cdot M} \quad (3)$$

Where E is the energy density in Wh Kg<sup>-1</sup>, C is the specific capacitance in F g<sup>-1</sup>, V<sub>2</sub> is the maximum potential after deducting the ohmic drop, V<sub>1</sub> is the minimum potential in volts, M is the mass of active mass in g and dV/dt is the slope of the discharge curve.

$$P = \frac{E}{\Delta t_d} \times 3600 \quad (4)$$

Where P is the power density in W Kg<sup>-1</sup>, E is the energy density in Wh Kg<sup>-1</sup> and t<sub>d</sub> is the discharge time in seconds.

**Table S1.** Textural properties of the synthesized porous carbon materials in a powder state by N<sub>2</sub> adsorption.

Sample	V <sub>micro</sub> (cm <sup>3</sup> g <sup>-1</sup> )	V <sub>meso</sub> (cm <sup>3</sup> g <sup>-1</sup> )	V <sub>t</sub> (cm <sup>3</sup> g <sup>-1</sup> )
ND1-CsCl-T	0.86	0.21	1.07
ND2-CsCl-T	0.81	0.22	1.03
ND4-CsCl-T	0.64	0.25	0.89
ND1-LiCl-T	0.48	0.59	1.07
ND1-LiNaCl-T	0.41	0.37	0.78
ND1-CsLiNaCl-T	0.77	0.22	0.99

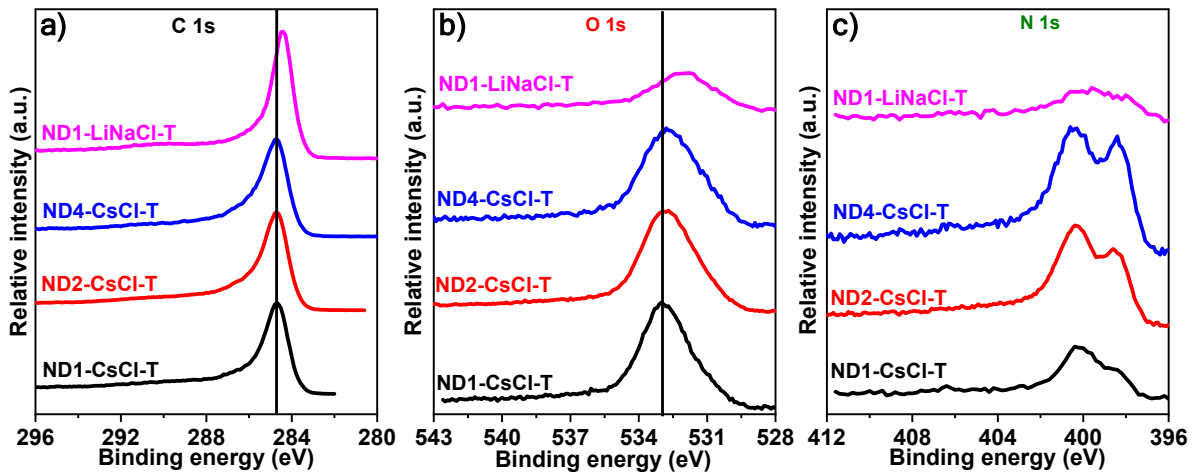


**Figure S1.** C 1s (a); O 1s (b); and N1s (c) high resolution XPS spectra of ND1-CsCl-T, ND2-CsCl-T, ND4-CsCl-T and ND1-LiNaCl-T.

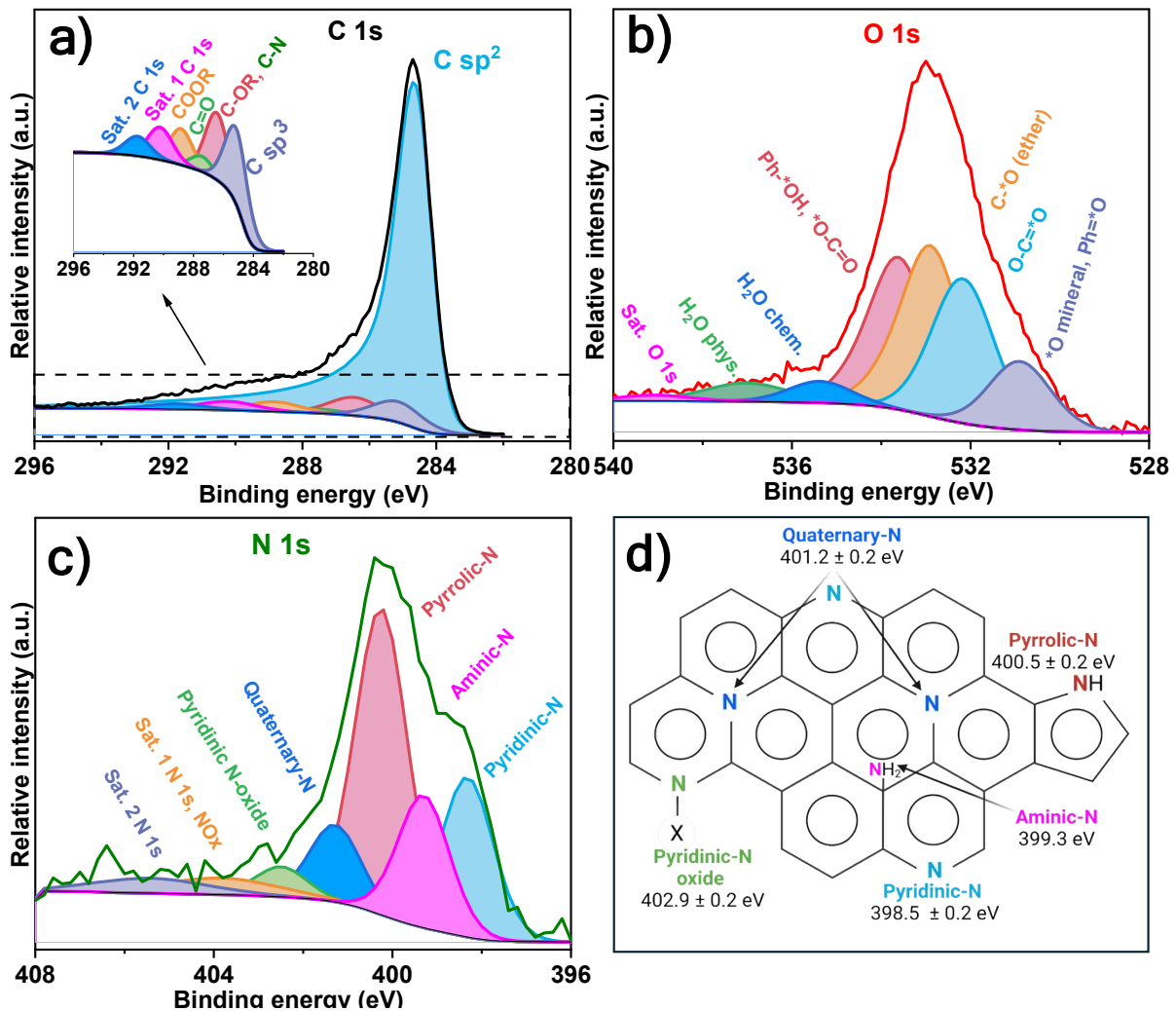


**Figure S2.** High-resolution XPS spectra deconvolution of ND1-CsCl-T : C 1s (a); O 1s (b); and N 1s (c); schematic representation of N-doped carbon, illustrating nitrogen surface groups, created by the authors with [Biorender.com](#) (d).

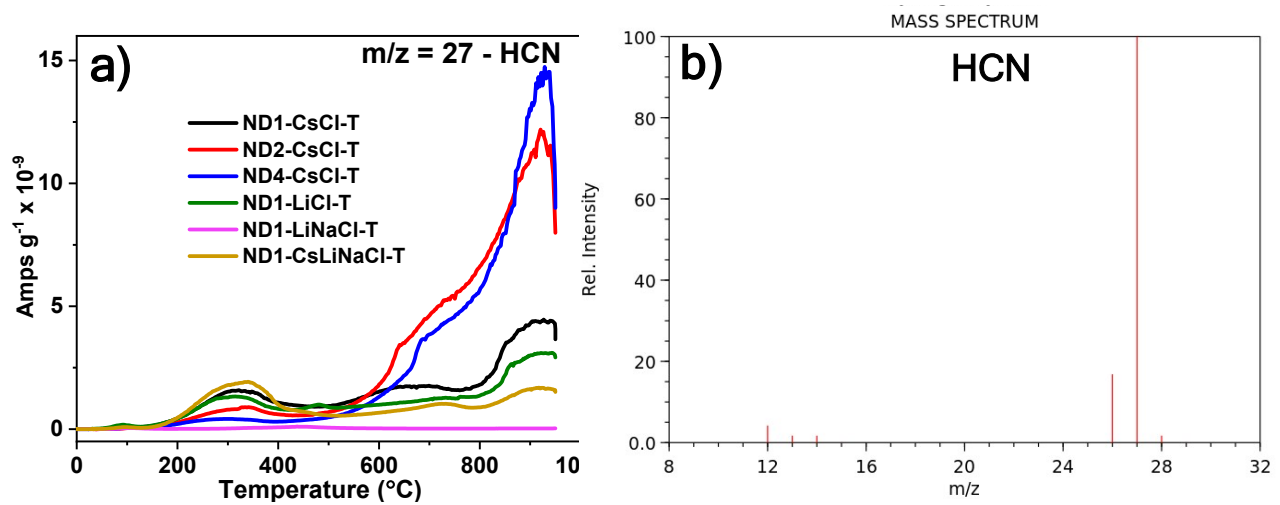


**Figure S3.** TPD-MS of HCN profiles for NDPC materials (a); mass spectra of HCN (source: NIST Chemistry WebBook, <https://webbook.nist.gov/chemistry>) (b).

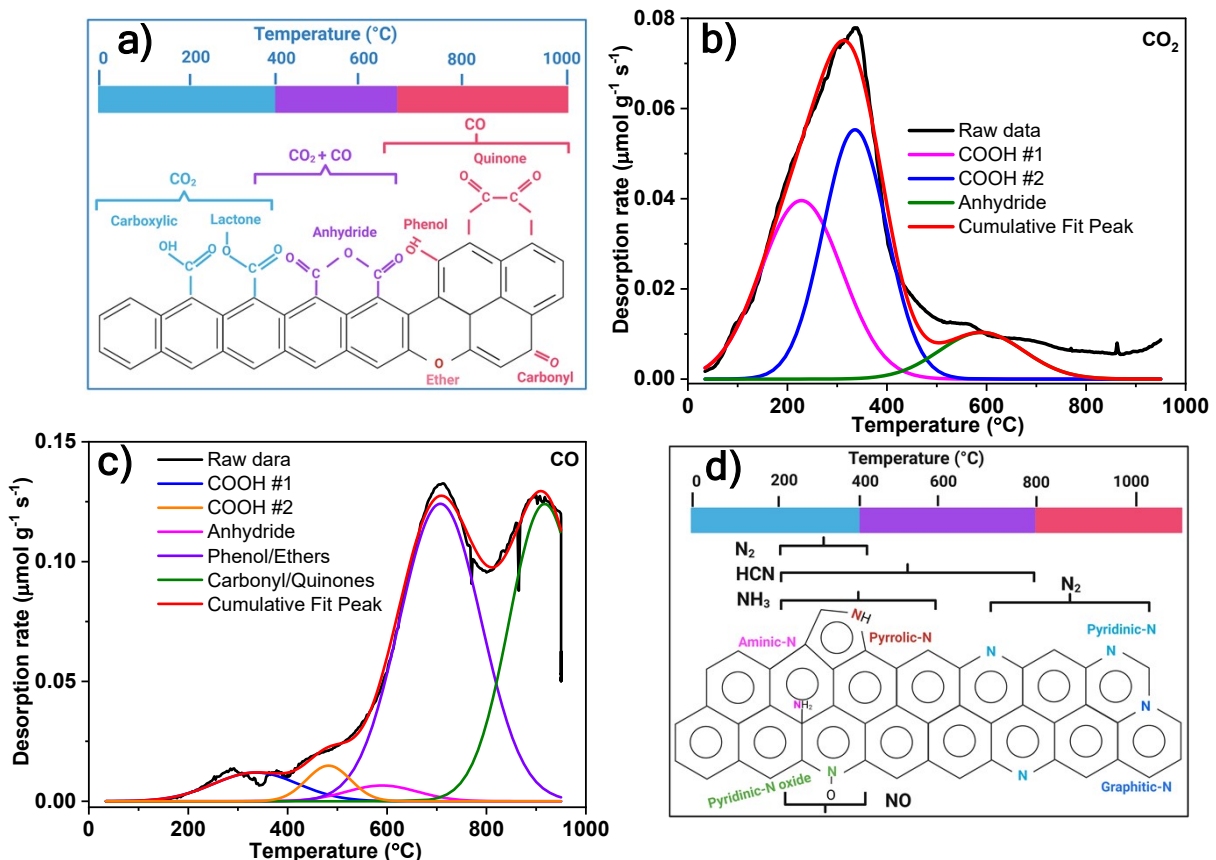


**Figure S4.** Typical oxygen functional groups present on the NDPC materials porous carbon surface and the corresponding CO and  $\text{CO}_2$  gases released after their thermal decomposition according to the TPD-MS,<sup>10</sup> created by the authors with <https://www.biorender.com> (a); deconvolution of the  $\text{CO}_2$  (b); and CO (c) gas profiles into the corresponding O-functional groups for ND1-LiNaCl-T; nitrogen functional groups present on the carbon surface and their thermal decomposition gases by TPD-MS (d), created by the authors with <https://www.biorender.com>.

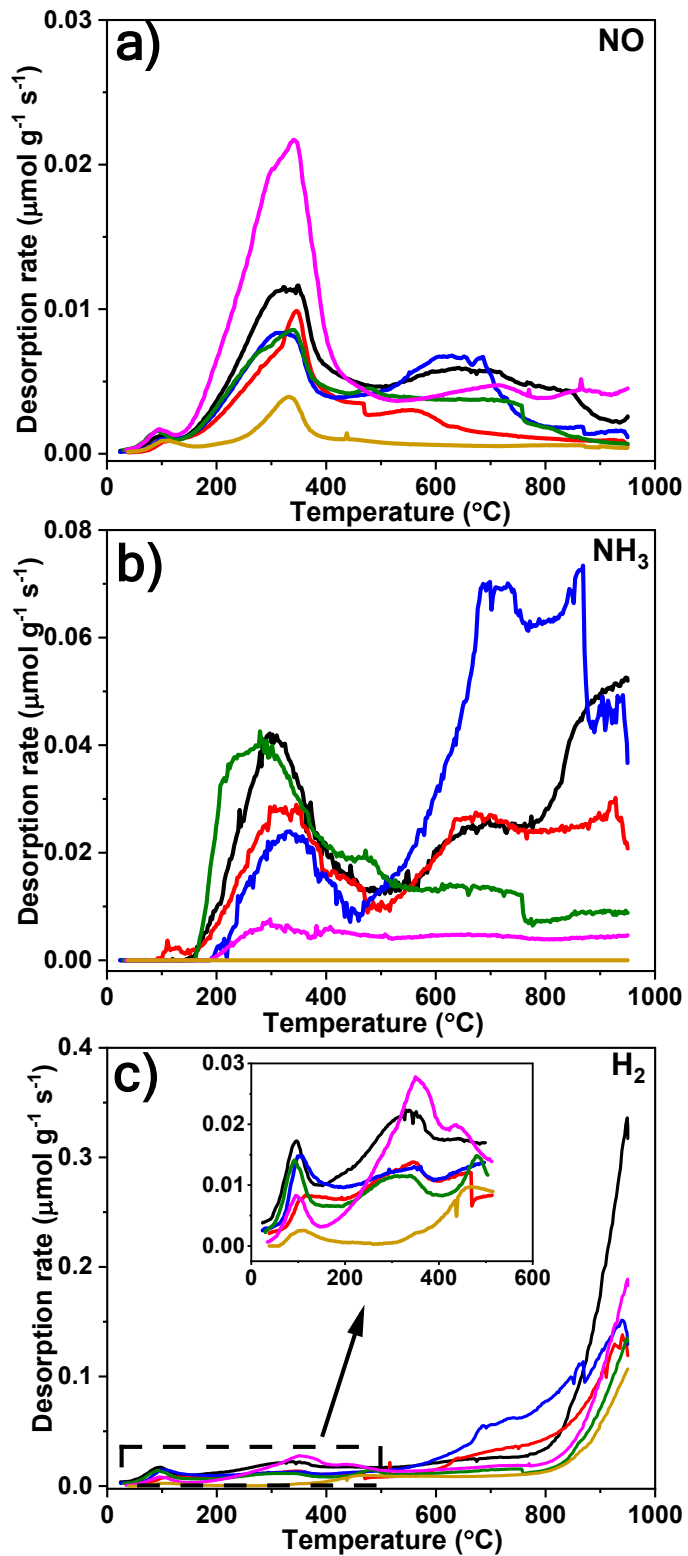


**Figure S5.** TPD-MS gas desorption profiles of NDPC materials showing desorption of NO (a); NH<sub>3</sub> (b); H<sub>2</sub> (c).

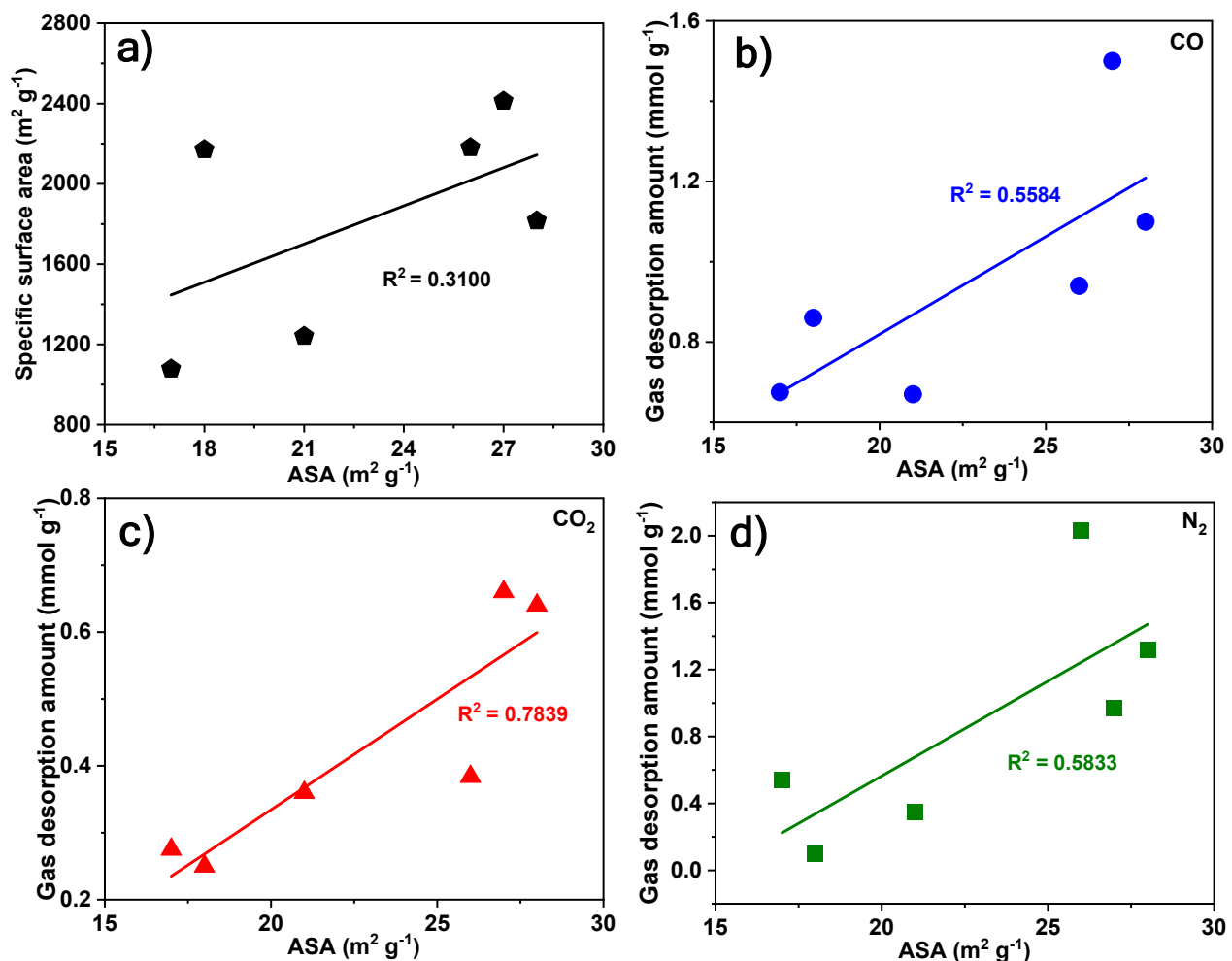


**Figure S6.** Plot of the specific surface area against the active surface area of the NDPC materials (a); linear correlation between the active surface area and the gas desorbed amount of CO (b);  $\text{CO}_2$  (c); and  $\text{N}_2$  (d).

**Table S2.** Summary of the electrochemical performance of the materials, based on half-cell results obtained from GCD and CV measurements.

The values in the table are reported in  $\text{mAh g}^{-1}$ , except for the last column which represents % Capacity Retention (CR).

Samples	$0.05 \text{ A g}^{-1}$	$0.1 \text{ A g}^{-1}$	$5 \text{ A g}^{-1}$	$10 \text{ A g}^{-1}$	$0.1 \text{ mVs}^{-1}$	$1 \text{ mVs}^{-1}$	$50 \text{ mVs}^{-1}$	$100 \text{ mVs}^{-1}$	% CR @ $100 \text{ mVs}^{-1}$
ND1-CsCl-T	159	148	3	0	181	157	41	26	15
ND2-CsCl-T	139	131	0	0	167	140	38	22	14
ND4-CsCl-T	122	117	0	0	147	124	38	23	19
ND1-LiCl-T	92	85	3	0	102	90	38	26	25
ND1-LiNaCl-T	83	78	14	1	106	81	30	21	30
ND1-CsLiNaCl-T	142	131	2	0	164	140	43	28	16

**Table S3.** Comparison of electrochemical performance of porous carbon-based cathodic half cells vs. Na metal at 0.1 A g<sup>-1</sup> current density from the literature.

Cathode materials	Electrolyte	Mass loading (mg cm <sup>-2</sup> )	SSA (m <sup>2</sup> g <sup>-1</sup> ) (N%)	Potential window (V)	Specific capacity (mAh g <sup>-1</sup> )
CSUN800 <sup>11</sup>	1 M NaPF <sub>6</sub> DME	0.7	2650 (6.4)	2 – 4	112
PDPC <sup>12</sup>	1 M NaClO <sub>4</sub> EC:DMC:EMC (1:1:1) 5.0% FEC	0.8 – 1 mg	-	2 – 4.3	123
NPC-60 <sup>13</sup>	1M NaClO <sub>4</sub> EC :DEC	1.5 – 6.0	1022.27 (4.7)	2 – 4.5	101
AJPC-M <sup>14</sup>	1 M NaPF <sub>6</sub> EC:DEC (1:1)	0.8	1529.75	1.5 – 3.3	70
AGLC <sup>15</sup>	1 M NaClO <sub>4</sub> EC:DEC (1:1) 2 vol% FEC	-	2961	2 – 4	71
NS-GHNS <sup>16</sup>	1 M NaClO <sub>4</sub> EC:DEC (1:1)	1.2 – 1.4	320 (3.34)	2.5 – 4.2	52 @ 0.2 A g <sup>-1</sup>

ANP <sup>17</sup>	1 M NaClO <sub>4</sub> EC:DEC (1:1)	1	2970 (0)	2 – 4.2	121
MERK-14 <sup>18</sup>	1 M NaClO <sub>4</sub> EC:DEC (1:1)	1.5 - 3	2286 (1.3)	1.5 – 4	136
CKNa-800mT <sup>19</sup>	1 M NaClO <sub>4</sub> EC:DEC (1:1)	2	2750 (0)	2 – 4	114
NHPC <sup>20</sup>	1 M NaPF <sub>6</sub> in 1:1 (EC:PC)	-	2225	1.5 – 4	63
CBC-C <sup>21</sup>	1 M NaClO <sub>4</sub> EC:DEC (1:1)	0.9	3229	2.7 – 4.2	47
PCC <sup>22</sup>	1 M NaClO <sub>4</sub> EC:DEC (1:1)	1	2325	2 – 4.2	95
ND1-CsCl-T*			2412 (3.4)		159
ND2-CsCl-T*	1 M NaPF <sub>6</sub> EC:DMC (1:1)	7 - 8	2181 (6.1) 1816 (8.0) 2171	1.5 – 4.5	139 122
ND1-CsLiNaCl-T*			2019		142
Kynol-5092-20*					103

\*This work

**Table S4.** Physico-chemical properties Kynol 5092–20 (provided by Kynol®), a commercial porous carbon cloth, extracted from our recent studies.<sup>5</sup>

S/N	Properties	Kynol 5092-20
1	Specific surface area ( $\text{m}^2 \text{ g}^{-1}$ )	2019
2	$L_0$ (nm)	0.94
3	$V_{\text{micro}}$ ( $\text{cm}^3 \text{ g}^{-1}$ )	0.82
4	$V_{\text{meso}}$ ( $\text{cm}^3 \text{ g}^{-1}$ )	0.05
5	$V_{\text{total}}$ ( $\text{cm}^3 \text{ g}^{-1}$ )	0.87
6	CO (mmol $\text{g}^{-1}$ )	0.41
7	$\text{CO}_2$ (mmol $\text{g}^{-1}$ )	~ 0.10
8	ASA ( $\text{m}^2 \text{ g}^{-1}$ )	20

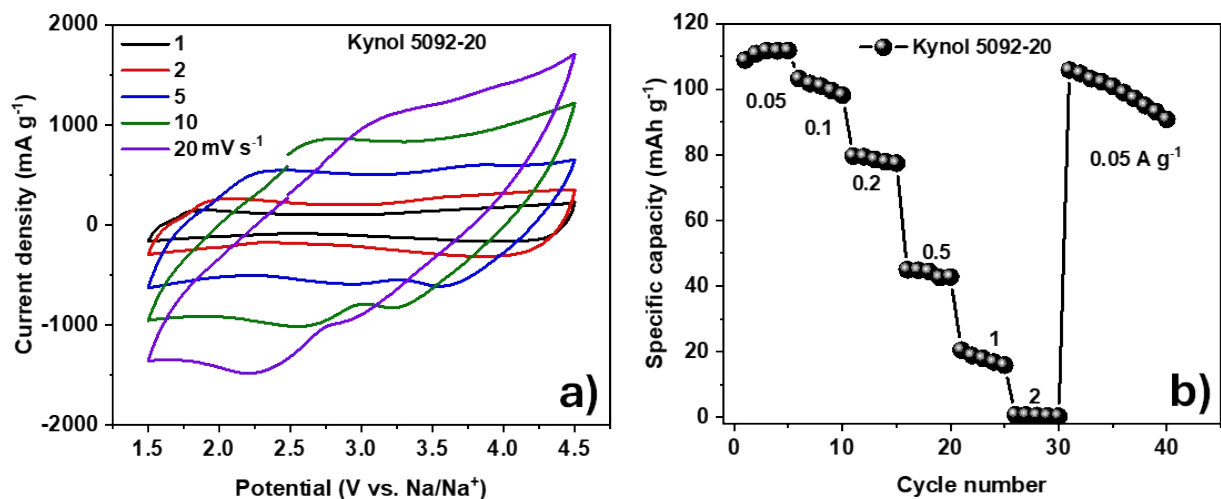


**Figure S7.** Electrochemical performance of Kynol 5092–20 in Na metal half cells, presenting the CV curve (a) and GCD (b). The activated carbon was directly used as a self-standing electrode, without binder or carbon black additives. It was tested in half vs. sodium metal in 1 M  $\text{NaPF}_6$  EC:DMC (1:1) electrolyte, within a potential range of 1.5 – 4.5 V, with a mass of loading 14.9  $\text{mg cm}^{-2}$  and an electrode diameter of 11 mm.

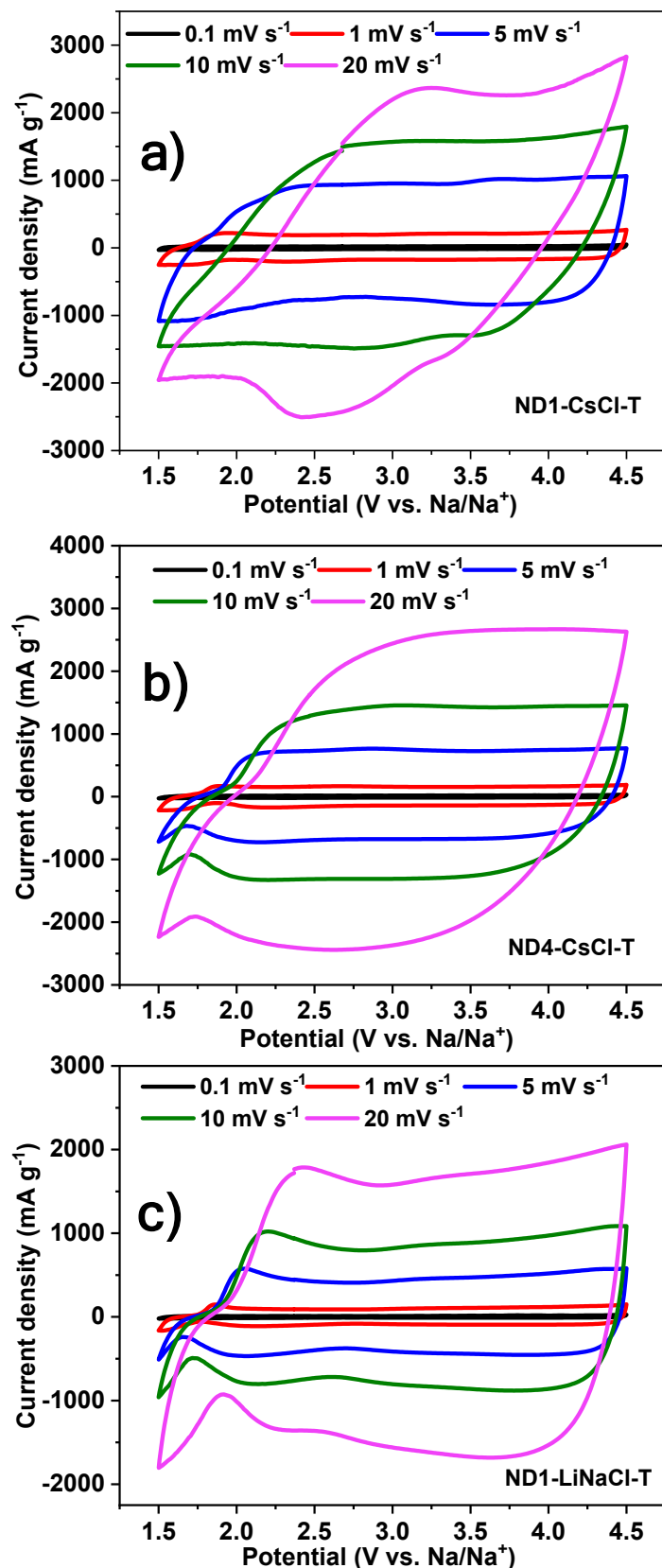


**Figure S8.** CV Curves for NDPC materials at various scan rates ( $0.1 - 20 \text{ mV s}^{-1}$ ) for ND1-CsCl-T (a); ND4-CsCl-T (b) and ND1-LiNaCl-T (c).

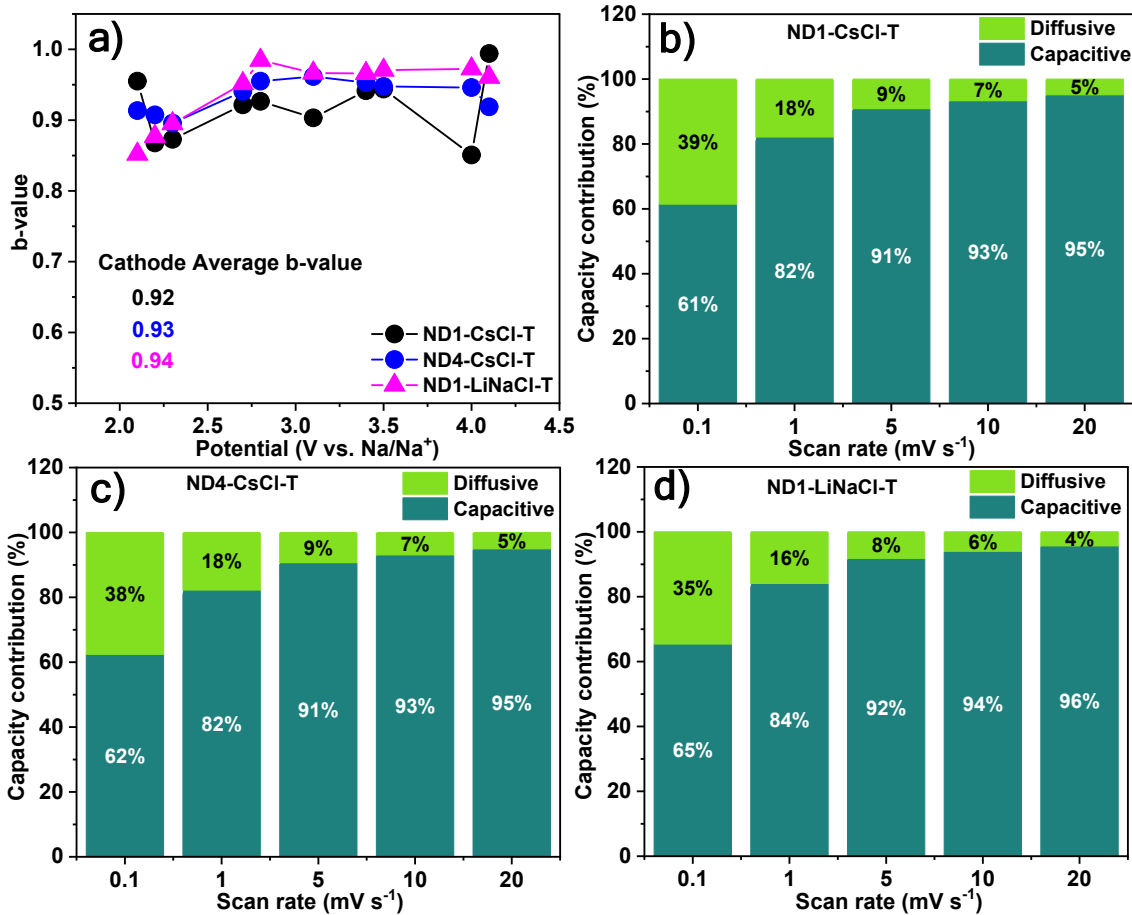


**Figure S9.** Graph depicting the b value as a function of voltage potential for the cathodic peak, including the average b value for ND1-CsCl-T, ND4-CsCl-T, and ND1-LiNaCl-T (a); Analysis of the diffusive and capacitive contributions to the total current at different scan rates for ND1-CsCl-T (b); ND4-CsCl-T (c); ND1-LiNaCl-T (d).

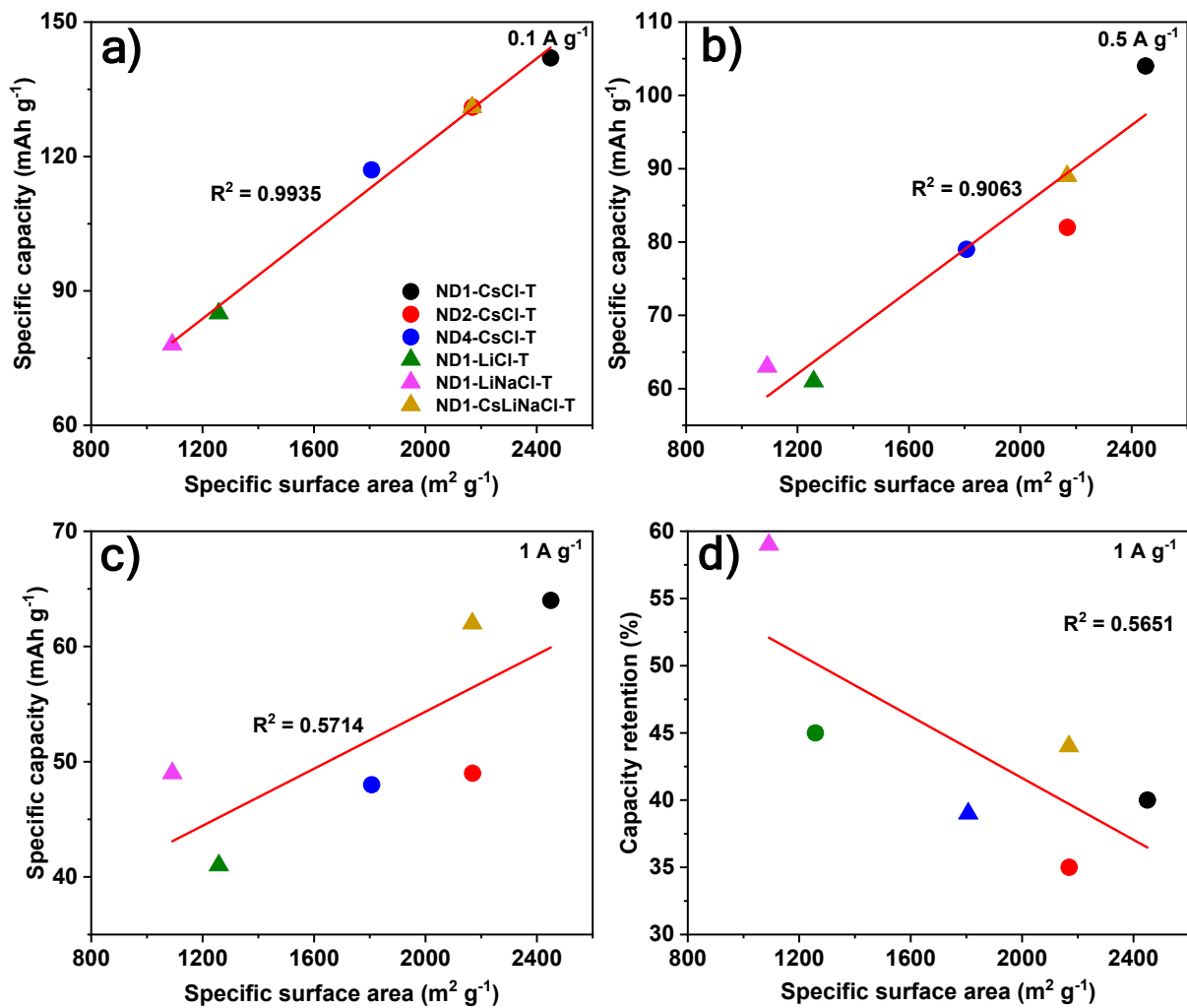


**Figure S10.** Plot of the specific capacity from GCPL versus the specific surface area at current density of 0.1 A g<sup>-1</sup> (a) 0.5 A g<sup>-1</sup> (b) and 1 A g<sup>-1</sup> (c); Plot of the capacity retention against the specific surface area at 1 A g<sup>-1</sup> (d).

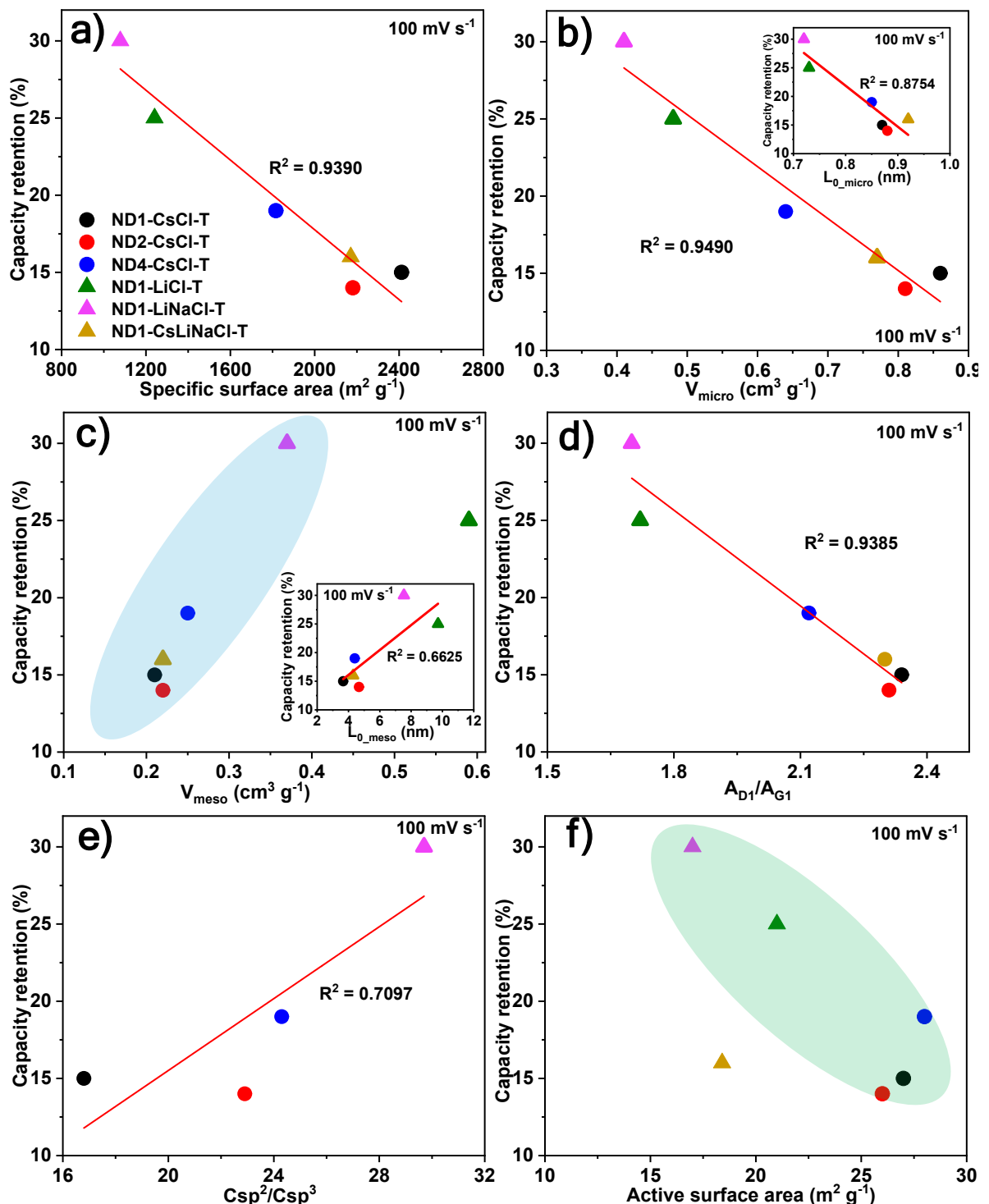


**Figure S11.** Capacity retention represented as a function of textural properties, specific surface area (a); volume of micropores with average micropores diameter inset (b); volume of mesopores with average mesopores diameter inset (c); structural properties, area ratio of  $D_1$  and  $G_1$  (d);  $Csp^2/Csp^3$ (e); and active surface area (f).

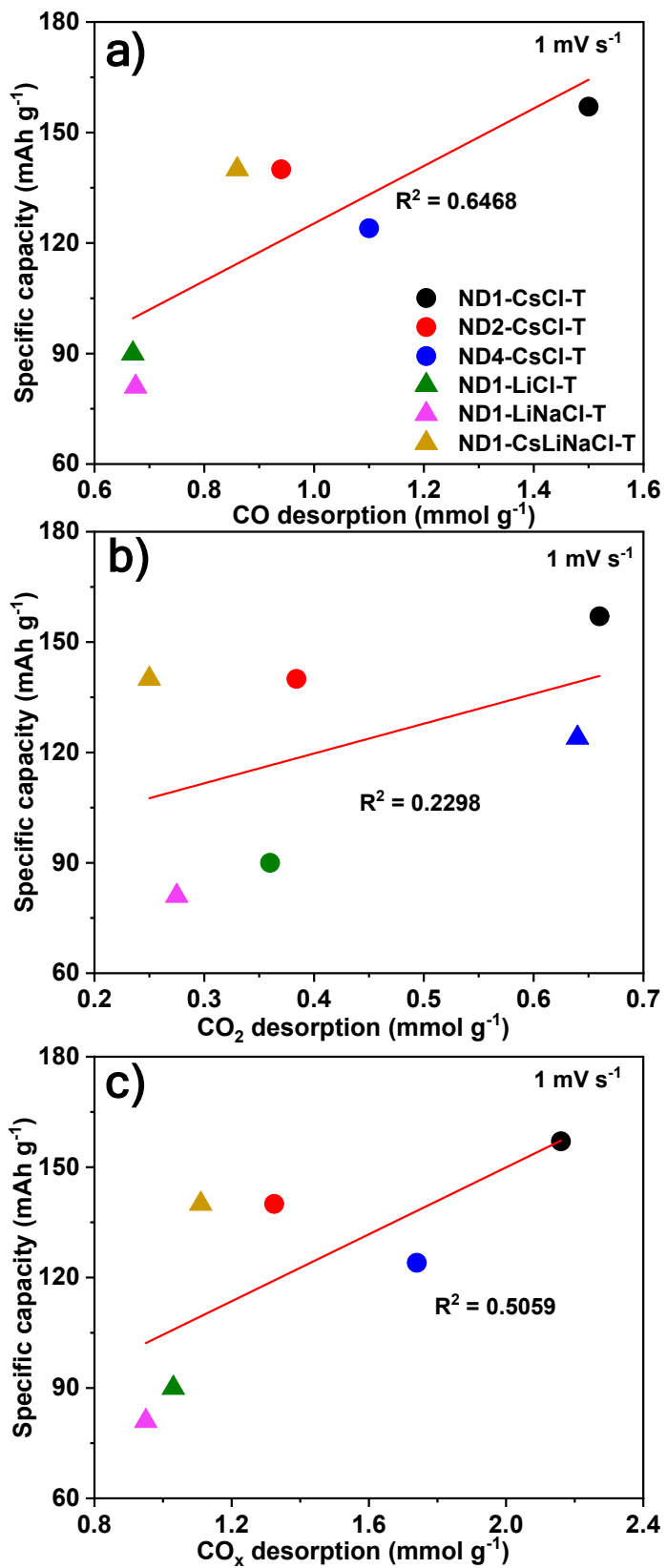


**Figure S12.** Specific capacity as a function of total CO desorption amount (a); total  $\text{CO}_2$  desorption amount (b); total  $\text{CO}_x$  ( $\text{CO} + \text{CO}_2$ ) desorption amount (c).

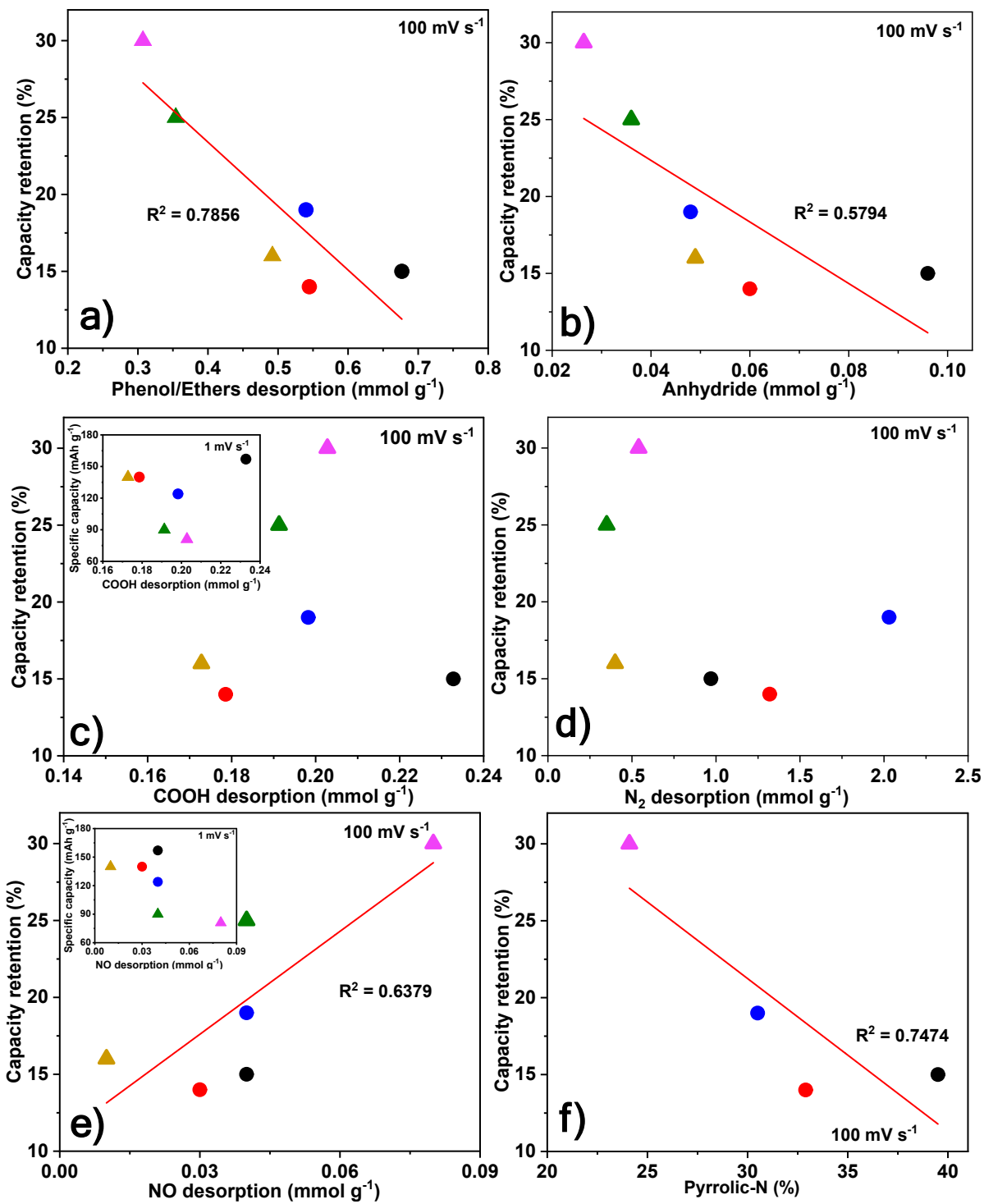


**Figure S13.** Capacity retention represented as a function of surface chemical groups, phenol/ethers (a) anhydride (b) COOH (with specific capacity inset) (c); N<sub>2</sub> (d); NO (with specific capacity inset) (e); and pyrrolic-N (f).

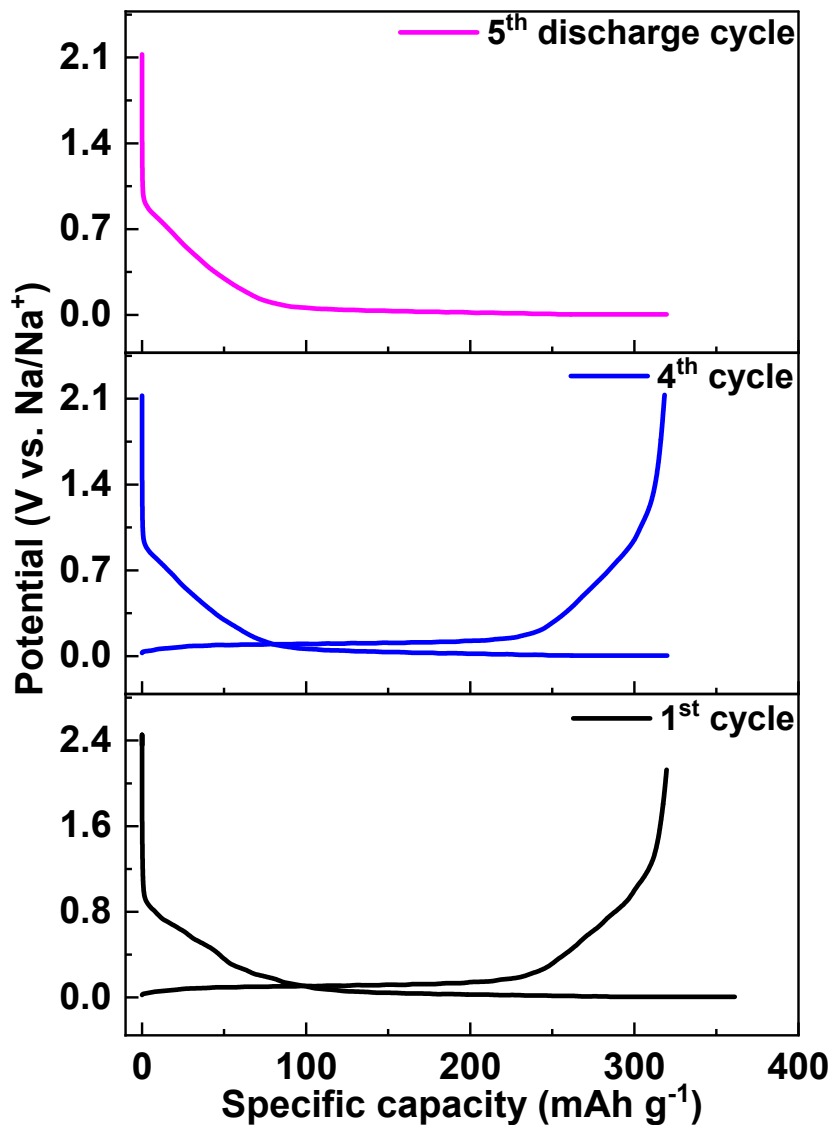


**Figure S14.** HC-R-St anode presodiation at C/10 (1C = 372 mAh g<sup>-1</sup>) for five cycles under constant current-constant voltage testing conditions.

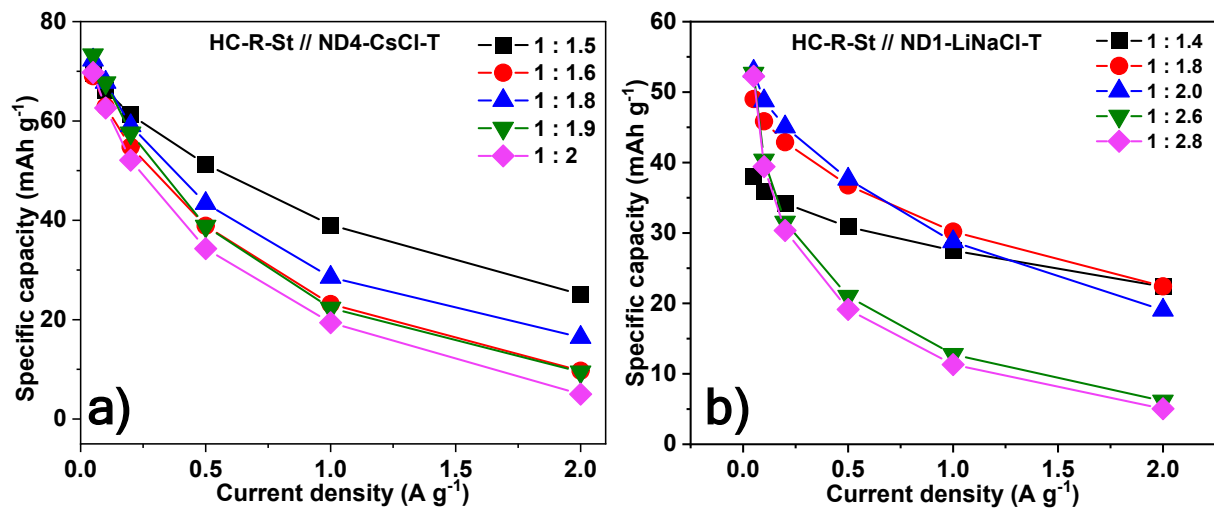


**Figure S15.** Plot showing the specific capacity as a function of current density for the optimized HC-R-St (anode) // ND4-CsCl-T (cathode) ratio (a) and HC-R-St (anode) // ND1-LiNaCl-T (cathode) ratio (b).

**Table S5.** Comparison of electrochemical performance of NDPC full cell with dual carbon sodium-ion capacitors from the literature at a current density of 0.1 A g<sup>-1</sup>.

Anode // Cathode	Potential window (V)	Electrolyte	Specific capacity (mAh g <sup>-1</sup> )
AGS-650//AGA-850 <sup>23</sup>	1 – 4	1 M NaClO <sub>4</sub> EC:DEC (1:1)	49 - 50
JPC-D//APJC-M <sup>14</sup>	0.15 – 3.29	1 M NaPF <sub>6</sub> EC:DEC (1:1)	43 (0.3 A g <sup>-1</sup> )
PFC//PFAC <sup>24</sup>	0 – 4	1 M NaClO <sub>4</sub> EC:DMC (1:1)	45.7 F g <sup>-1</sup>
MDC//K-MDC <sup>25</sup>	0 – 4	1 M NaClO <sub>4</sub> EC:DEC (1:1)	49
Mo <sub>2</sub> C/C-2//PC <sup>26</sup>	0 – 4	-	56.9 F g <sup>-1</sup>
Sb@NC//PDPC <sup>27</sup>	1 – 4	1 M NaClO <sub>4</sub> EC:DMC:EMC (1:1:1) 5.0% FEC	60.2
PNPOC-800//APNPOC-800 <sup>28</sup>	0 – 4	1 M NaPF <sub>6</sub> EC:DEC (1:1)	48.65 F g <sup>-1</sup>
SCNP//ANP <sup>17</sup>	1 – 4	1 M NaClO <sub>4</sub> EC:DEC (1:1)	50
HAT-CNF//STC-16 <sup>29</sup>	0.5 – 4	1 M NaClO <sub>4</sub> EC:PC:FEC (45:45:10, mass)	55.8 F g <sup>-1</sup>
HC-R-St//ND4-CsCl-T (1:1.5)*	1.5 – 4.5	1 M NaPF <sub>6</sub> EC:DMC (1:1)	66 (83.5 F g <sup>-1</sup> )

\*This work

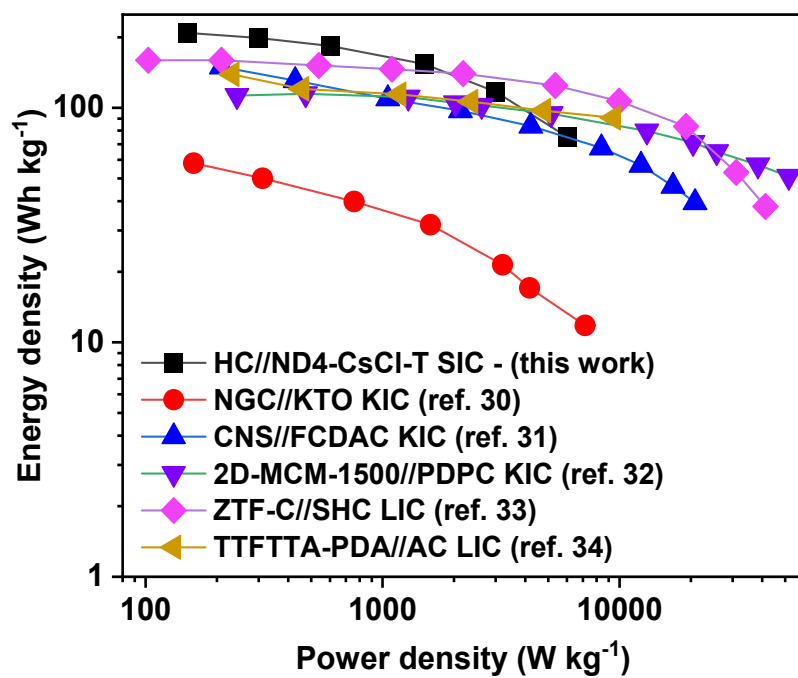


**Figure S16.** Evaluation of the energy and power density of the sodium-ion capacitor compared to other hybrid technology (potassium/lithium-ion capacitor) in the literature.<sup>30–34</sup>

**Table S6.** Comparison of electrochemical performance of dual carbon-based sodium-ion capacitors and other hybrid metal ion based technology reports from the literature. The table includes data on energy density (ED, Wh kg<sup>-1</sup>) and power density (PD, W kg<sup>-1</sup>).

Anode // Cathode	Materials type	Potential window (V)	Electrolyte	Maximum ED	Maximum PD	Cycling stability
<b>SIC – Carbon Anode // Carbon Cathode</b>						
HC-R-St//ND4-CsCl-T (1:1.5) – this work	hard carbon // porous carbon	1.5 – 4.5	1 M NaPF <sub>6</sub> EC:DMC (1:1)	209@150	75@6000	80% @4200 cyles@0.1 A g <sup>-1</sup>
MER1200//MERK14 <sup>18</sup>	hard carbon // porous carbon	1 – 4	1 M NaClO <sub>4</sub> EC:DEC (1:1)	195.4@85	72.3@13800	91.2% @16000 cyles@5 A g <sup>-1</sup>
RGO400//RGO400 <sup>35</sup>	reduced graphene oxide // reduced graphene oxide	1 – 4	1 M NaPF <sub>6</sub> DME	91@631	48@10896	98% @1800 cyles@5 A g <sup>-1</sup>
AGS-650//AGA-850 <sup>23</sup>	carbon sponges // porous carbon	1 – 4	1 M NaClO <sub>4</sub> EC:DEC (1:1)	120@250	72@24400	78% @10000 cyles@2 A g <sup>-1</sup>
JPC-D//APJC-M <sup>14</sup>	hard carbon // porous activated carbon	0.15 – 3.29	1 M NaPF <sub>6</sub> EC:DEC (1:1)	86@636	16@3440	92% @1000 cyles@1.2 A g <sup>-1</sup>
PFC//PFAC <sup>24</sup>	porous framework carbon // porous framework activated carbon	0 – 4	1 M NaClO <sub>4</sub> EC:DMC (1:1)	101.6@200	51.1@20000	71.8% @10000 cyles@2 A g <sup>-1</sup>
MDC//K-MDC <sup>25</sup>	metal–azolate framework-6s-derived carbons // KOH-assisted pyrolysis of MDCs	0 – 4	1 M NaClO <sub>4</sub> EC:DEC (1:1)	100@200	53.2@20000	80% @1000 cyles@1 A g <sup>-1</sup>
PNPOC-800//APNPOC-800 <sup>28</sup>	N, P, O ternary-doped	0 – 4	1 M NaPF <sub>6</sub> EC:DEC	105.48@185	37.58@13590	87.43% @9000 cyles@1 A g <sup>-1</sup>

				(1:1)		
SCNP//ANP <sup>17</sup>	mesoporous carbon // alkaline-activated PNPOC-800 S-doped carbon nanoparticles // activated nanoparticles Ordered microporous carbon	1 – 4	1 M NaClO <sub>4</sub> EC:DEC (1:1)	105@185	69@25000	76% @10000 cyles@2 A g <sup>-1</sup>
OMC//N-OMC <sup>36</sup>	nitrogen-doped ordered microporous carbon Microporous nitrogen-rich carbon fibers // Salt-templated carbon	0 – 4	1 M NaClO <sub>4</sub> EC:PC (1:1) 5.0% FEC	119@73	31@5807	85% @1800 cyles@5 A g <sup>-1</sup>
HAT-CNF//STC-16 <sup>29</sup>	N-doped carbon // Activated carbon	0.5 – 4	1 M NaClO <sub>4</sub> EC:PC:FEC (45:45:10, mass)	95@190	18@13000	90% @1000 cyles@1 A g <sup>-1</sup>
As8Mg//AC <sup>37</sup>	P,N-Doped Interconnected Carbon Nanosheets with Hierarchical Porosity using KCl/Ice As Dual-Templates // KOH-treated N-doped carbon nanosheets	0.5 – 4	1 M NaPF <sub>6</sub> EC:DEC (30:70, vol%)	224@53	51@10410	99.7% @600 cyles@0.2 A g <sup>-1</sup>
P,N-HPCNS-KCl/Ice//N-PCNS-KOH <sup>38</sup>		0 – 4	1 M NaClO <sub>4</sub> EC:PC:FEC (1:1:0.05, vol%)	135.3@30	40@16100	88.6% @8000 cyles@5 A g <sup>-1</sup>

**SIC – Carbon composite Anode // Carbon Cathode**

	Molybdenum carbide/carbon composite // porous carbon	0 – 4	-	50.2@200	16.7@10000	77.5% @1800 cyles@5 A g <sup>-1</sup>
Mo <sub>2</sub> C/C-2//PC <sup>26</sup>	Vanadium Nitride Quantum Dots Modified One-Dimensional Carbon Cages // Activated N/F co-doped carbon nanofiber cages	0 – 4	-	198.8@157	95@9100	73.5% @8000 cyles@1 A g <sup>-1</sup>
VNQDs@PCNFs-N/F//APCNFs-N/F <sup>39</sup>	Sb-carbon composite // Polyaniline-Derived Porous Carbon	1 – 4	1 M NaClO <sub>4</sub> EC:DMC:E MC (1:1:1) 5.0% FEC	157@230	49@25000	80% @4000 cyles@2 A g <sup>-1</sup>
Sb@NC//PDPC <sup>27</sup>	In <sub>6</sub> S <sub>7</sub> /nitrogen and sulfur co-doped carbon hollow microspindles // polyaniline derived porous carbon	1 – 3.8	1 M NaPF <sub>6</sub> in DME	136.3@473.6	52.1@47466	68.5% @20000cycles@5 A g <sup>-1</sup>
In <sub>6</sub> S <sub>7</sub> /NSC HMS//PDPC <sup>40</sup>	<b>Potassium-ion capacitor (KIC)</b>					
KTO // NGCC <sup>30</sup>	K <sub>2</sub> Ti <sub>6</sub> O <sub>13</sub> (KTO) microscaffolds // N-doped nanoporous graphenic carbon	0 – 3.5	1 M KPF <sub>6</sub> PC (5% FEC)	58.2@160	12@7200	75.5% @ 5000 cycles @1 A g <sup>-1</sup>
CNS//FCDAC KIC <sup>31</sup>	Carbon nanosheets // framework carbon derived activated carbon	0 – 4.2	0.8 M KPF <sub>6</sub> EC:DEC (1:1, v/v)	149@210	40@21000	80% @ 5000 cycles @2 A g <sup>-1</sup>

2D-MCM-1500//PDPC KIC <sup>32</sup>	Two-dimensional mesoporous carbon microcoins (2D-MCMs) // Polyaniline-derived porous carbon	1 – 4.06	3 M KFSI EC:DEC (1:1 v/v)	113@495	51.25@5100 0	73% @ 10000 cycles @2 A g <sup>-1</sup>
<b>Lithium-ion capacitor (LIC)</b>						
SHC//ZTF-C LIC <sup>33</sup>	Sucrose hard carbon // zinc 2,3,5,6-tetrafluoroterephthalic derived carbon	1.5 – 4	1 M LiPF <sub>6</sub> EC:DEC:DMC (1:1:1 in vol%)	157@103.7	37.3@40000	85% @ 5000 cycles @5 A g <sup>-1</sup>
TTFTTA-PDA//AC LIC <sup>34</sup>	Tetrathiafulvalene tetrathiophenal p-phenylenediamine // Activated carbon	2 - 4	1 M LiPF <sub>6</sub> EC:DEC (1:1, vol%)	140@233	91@9328	81.3% @ 42200 cycles @4 A g <sup>-1</sup>

## References

- 1 J. Jagiello, A. Chojnacka, S. E. M. Pourhosseini, Z. Wang and F. Beguin, *Carbon*, 2021, **178**, 113–124.
- 2 A. Platek-Mielczarek, C. Nita, C. Matei Ghimbeu, E. Frackowiak and K. Fic, *ACS Appl. Mater. Interfaces*, 2021, **13**, 2584–2599.
- 3 A. Beda, C. Vaulot, F. Rabuel, M. Morcrette and C. M. Ghimbeu, *Energy Advances*, 2022, **1**, 185–190.
- 4 R. P. Rocha, M. F. R. Pereira and J. L. Figueiredo, *Catalysis Today*, 2023, **418**, 114136.
- 5 B. Réty, H.-Y. Yiin and C. M. Ghimbeu, *Energy Storage Materials*, 2025, **74**, 103963.
- 6 J. Wang, J. Polleux, J. Lim and B. Dunn, *J. Phys. Chem. C*, 2007, **111**, 14925–14931.
- 7 P. Cai, K. Zou, X. Deng, B. Wang, M. Zheng, L. Li, H. Hou, G. Zou and X. Ji, *Advanced Energy Materials*, 2021, **11**, 2003804.
- 8 S. Payá, M. D. Casal, N. Díez and M. Sevilla, *Carbon*, 2025, **235**, 120056.
- 9 K. Zou, P. Cai, C. Liu, J. Li, X. Gao, L. Xu, G. Zou, H. Hou, Z. Liu and X. Ji, *J. Mater. Chem. A*, 2019, **7**, 13540–13549.
- 10 J. L. Figueiredo, M. F. R. Pereira, M. M. A. Freitas and J. J. M. Órfão, *Carbon*, 1999, **37**, 1379–1389.
- 11 Z. Yang, X. Liu, X. Ma, T. Cao, J. Xu, H. Feng, R. Diao, F. Qi, H. Huang and P. Ma, *Advanced Functional Materials*, 2024, **34**, 2310717.
- 12 W. Yu, C. Zhu, R. Wang, J. Chen, Q. Liu, S. Zhang, S. Zhang, J. Sun and L. Yin, *Energy & Environmental Materials*, 2023, **6**, e12337.
- 13 P. Cai, R. Momen, M. Li, Y. Tian, L. Yang, K. Zou, X. Deng, B. Wang, H. Hou, G. Zou and X. Ji, *Chemical Engineering Journal*, 2021, **420**, 129647.
- 14 Nagmani, B. Kanta Satpathy, A. Kumar Singh, D. Pradhan and S. Puravankara, *New Journal of Chemistry*, 2023, **47**, 12658–12669.
- 15 D. Qiu, C. Yue, C. Qiu, L. Xian, M. Li, F. Wang and R. Yang, *Electrochimica Acta*, 2022, **405**, 139791.
- 16 R. Thangavel, A. G. Kannan, R. Ponraj, G. Yoon, V. Aravindan, D.-W. Kim, K. Kang, W.-S. Yoon and Y.-S. Lee, *Energy Storage Materials*, 2020, **25**, 702–713.
- 17 N. Diez, M. Sevilla and A. B. Fuertes, *Carbon*, 2023, **201**, 1126–1136.
- 18 S. Liu, C. Song, W. Zhang, T. Zhang, W. Shao, Z. Weng, M. Yao, H. Huang, X. Jian and F. Hu, *Chemical Engineering Journal*, 2022, **450**, 138103.
- 19 M. D. Casal, N. Diez, S. Payá and M. Sevilla, *ACS Applied Energy Materials*, 2023, **6**, 8120–8131.
- 20 J. Ajuria, E. Redondo, M. Arnaiz, R. Mysyk, T. Rojo and E. Goikolea, *Journal of Power Sources*, 2017, **359**, 17–26.
- 21 Y. Guo, W. Liu, R. Wu, L. Sun, Y. Zhang, Y. Cui, S. Liu, H. Wang and B. Shan, *ACS Appl. Mater. Interfaces*, 2018, **10**, 38376–38386.
- 22 A. Fombona-Pascual, N. Diez, A. B. Fuertes and M. Sevilla, *ChemSusChem*, 2022, **15**, e202201046.
- 23 S. Payá, N. Díez and M. Sevilla, *Sustainable Energy Fuels*, 2023, **7**, 2378–2389.
- 24 C. Li, K. Cao, Y. Fan, Q. Li, Y. Zhang and Z. Guo, *Journal of Colloid and Interface Science*, 2023, **652**, 1356–1366.
- 25 Y. M. Jung, J. H. Choi, D. W. Kim and J. K. Kang, *Advanced Science*, 2023, **10**, 2301160.
- 26 M. Jia, J. Wei, Y. Zhang, L. Hou, J. Sun and C. Yuan, *Nanoscale*, 2023, **15**, 15334–15343.
- 27 W.-Q. Yu, C.-Y. Zhu, R.-T. Wang, J.-C. Chen, Q.-Y. Liu, S.-X. Zhang, Z.-J. Gao, C.-X. Wang, Z.-W. Zhang and L.-W. Yin, *Rare Met.*, 2022, **41**, 3360–3369.
- 28 C. Wang, Q. Yu, N. Zhao, B. Li, W. Shen, F. Kang, Z.-H. Huang and R. Lv, *Journal of Materomics*, 2022, **8**, 1149–1157.

- 29 R. Yan, E. Josef, H. Huang, K. Leus, M. Niederberger, J. P. Hofmann, R. Walczak, M. Antonietti and M. Oschatz, *Adv. Funct. Mater.*, 2019, **29**, 1902858.
- 30 S. Dong, Z. Li, Z. Xing, X. Wu, X. Ji and X. Zhang, *ACS Appl. Mater. Interfaces*, 2018, **10**, 15542–15547.
- 31 J. Chen, B. Yang, H. Hou, H. Li, L. Liu, L. Zhang and X. Yan, *Advanced Energy Materials*, 2019, **9**, 1803894.
- 32 X. Huang, J. Gao, Y. Qin, D. Du, R. Liu, Y. Shi, C. Wang, Z. Zhang, J. Zhang, J. Sun, T. Li, L. Yin and R. Wang, *ACS Nano*, 2024, **18**, 21459–21471.
- 33 Z. Xu, J. Li, X. Li, Z. Chen, C. Chen, S. A. Ali Shah and M. Wu, *Applied Surface Science*, 2021, **565**, 150528.
- 34 Z.-M. Yang, Y. Wang, M.-H. Zhang, Z.-Y. Hou, S.-P. Zhao, X. Han, S. Yuan, J. Su, Z. Jin and J.-L. Zuo, *Energy Storage Materials*, 2025, **75**, 104038.
- 35 C. Zhang, P. Chandan Solanki, D. Cao, H. Zhao and Y. Lei, *ACS Appl. Mater. Interfaces*, 2023, **15**, 24459–24469.
- 36 J. Li, B. Wang, T. Hu, Y. Wang, Z. Sun, C. Wang, D. Zhang, Z. Wang and F. Li, *J. Mater. Chem. A*, 2021, **9**, 3360–3368.
- 37 C. Li, Z. Song, M. Liu, E. Lepre, M. Antonietti, J. Zhu, J. Liu, Y. Fu and N. López-Salas, *Energy & Environmental Materials*, 2024, **7**, e12695.
- 38 J. Niu, J. Guan, M. Dou, Z. Zhang, J. Kong and F. Wang, *ACS Applied Energy Materials*, 2020, **3**, 2478–2489.
- 39 J. Yuan, M. Qiu, X. Hu, Y. Liu, G. Zhong, H. Zhan and Z. Wen, *ACS Nano*, 2022, **16**, 14807–14818.
- 40 C. Zhu, W. Yu, S. Zhang, J. Chen, Q. Liu, Q. Li, S. Wang, M. Hua, X. Lin, L. Yin and R. Wang, *Advanced Materials*, 2023, **35**, 2211611.